Seed-Mediated Synthesis of Pd Nanocrystals: Factors Influencing a Kinetic- or Thermodynamic-Controlled Growth Regime

ARTICLE *in* THE JOURNAL OF PHYSICAL CHEMISTRY C · APRIL 2007

Impact Factor: 4.77 · DOI: 10.1021/jp0702752

6 AUTHORS, INCLUDING:

Gilles Berhault
French National Centre for Scientific Research
133 PUBLICATIONS **1,752** CITATIONS
SEE PROFILE

Denis Uzio
IFP Energies nouvelles
66 PUBLICATIONS **863** CITATIONS
SEE PROFILE

Seed-Mediated Synthesis of Pd Nanocrystals: Factors Influencing a Kinetic- or Thermodynamic-Controlled Growth Regime

Gilles Berhault,*,† Marta Bausach,† Laure Bisson,‡ Loïc Becerra,† Cécile Thomazeau,§ and Denis Uzio§

Institut de Recherches sur la Catalyse et l'Environnement de Lyon, UMR 5256 CNRS, Université Lyon I, 2 avenue Albert Einstein, 69100 Villeurbanne, France, Laboratoire de Chimie de la Matière Condensée de Paris, UMR 7574 CNRS, Université Pierre et Marie Curie Paris VI, 4 Place Jussieu, 75005 Paris, France, and IFP-Lyon, IFP, BP 3, 69390 Vernaison, France

Received: January 12, 2007; In Final Form: February 28, 2007

Palladium nanoparticles with defined morphologies were synthesized using a seed-mediated approach in the presence of cetyltrimethylammonium bromide (CTAB). This seeding technique, already applied to Ag and Au nanostructures, was successfully extended here to Pd, a noble metal with important applications in catalysis. Various types of morphologies were obtained going from 0-D nanocrystals (cubes, icosahedral multiply twinned particles) to 1-D (nanorods) and 2-D nanocrystals (triangular nanosheets). Palladium nanorods were obtained in a relatively high yield and present a well-defined 5-fold symmetry similar to that reported previously for Ag and Au. Embedding the $PdCl_4^{2-}$ precursor inside CTAB micelles was found to be a key parameter to decrease the rate of reduction of palladium and to allow a better kinetic-controlled growth regime, favoring the formation of nanorods. Shifting the experimental conditions to a thermodynamic-controlled growth regime also selectively led to the formation of cubic (∼80%) or icosahedral (∼100%) particles.

1. Introduction

Nanostructured metallic particles have generated, in the past decade, a great interest in materials science due to their unusual properties. Indeed, by finely tuning their size and/or shape, nanoscale metallic particles can present physical properties different from their bulk counterpart.[1,2]

A large effort has been devoted to the synthesis of rods and wires since these anisotropic particles exhibit promising applications in photonics,[3,4] catalysis,[5−9] electronic devices,[10] chemical sensing,[11] drug delivery,[12] and novel contrast agents.[13] In this respect, a great deal of studies has been triggered due to the possibility of tuning their optical properties through the control of their particle size and shape, particularly for Ag and Au.[14] Indeed, for these particles, the surface plasmon resonance (SPR) of the metal is split into two bands, a longitudinal plasmon band corresponding to light absorption and scattering along the long axis of the particle and a transverse plasmon band corresponding to absorption and scattering along the short axis of the rod.[15] Rod-like metallic particles could also exhibit strong enhanced surface Raman scattering (SERS) effects when molecules are adsorbed onto their surface due to coupling of the plasmon band of the metal with the molecules' electronic states.[16] Rods and wires have enhanced electric fields at their tips, which would favor an increase of the SERS activity (the "lightning rod" effect).[17,18] These anisotropic particles are, therefore, good candidates for application as optical sensors.[19] Nanostructured metallic particles are also interesting materials for catalytic applications.[20] Control of the shape of the nanoparticles may provide a way of preferentially exposing one particular type of crystallographic facet. This would lead to highly selective catalytic systems for structure-sensitive reactions.[5,6,21,22]

Different approaches have been developed to synthesize nanoscale materials such as lithography,[23] vapor−liquid−solid (VLS) growth techniques,[24] or electrochemical synthesis.[25] However, due to their relatively simple technics and low cost to produce at large-scale nanometric materials, chemical reduction of a metallic salt precursor has been successfully applied in the presence of a rigid or soft template or by using a seed-mediated approach.[26−29]

The anisotropic growth can be controlled through the selective adsorption of ions, surfactants, ligands, or polymers on specific crystallographic facets. Since the crystalline growth rate varies exponentially with the surface energy, the selective adsorption of an additive on a given crystallographic facet can inhibit the growth rate along one particular crystallographic direction, leading to a preferential growth along another (or other) direction(s) and to the formation of 1-D (rod-like) or 2-D (disks or plates) nanostructures. This methodology has been successfully applied in colloidal synthesis using two major strategies: in organic solvent, the polyol process using a polymer, generally poly(vinylpyrrolidone) (PVP), as a capping agent[30] or in aqueous solutions, through the use of a surfactant, generally cetyltrimethylammonium bromide (CTAB), playing both the role of capping and structure-directing agent.[31] In this latter case, better control of nucleation and growth steps can be achieved using seeds, that is, isotropic particles of 3−4 nm serving as nucleation sites for the anisotropic growth.

Noble metals are attractive candidates for shape-controlled synthesis due to their outstanding catalytic properties. However, up to now, the seeding approach has not been applied to Pd or Pt. Shape control over Pd or Pt nanoparticles was obtained using

* To whom correspondence should be addressed. Phone: +33-472-44-53-20. Fax: +33-472-44-53-99. E-mail: gilles.berhault@ircelyon.univ-lyon1.fr.

† Université Lyon I.

‡ Université Pierre et Marie Curie Paris VI.

§ IFP-Lyon.

10.1021/jp0702752 CCC: $37.00
Published on Web 04/03/2007

polymers as the capping agent. In this respect, Telkar et al. have synthesized Pd nanocubes using a polyol approach[21] following the initial work of Teranishi et al.[32] Similarly, Xia and co-workers have nicely shown that selective etching can induce the selective formation of single-crystalline Pd nanocubes.[33,34] Balint et al. have used NIPA (*N*-isopropylacrylamide) for synthesizing well-defined Pt nanoparticles, for example, cubes and prisms.[22] El-Sayed and co-workers have also established the link between nanomorphology and catalytic properties in colloidal conditions through the formation of tetrahedral and cubic nanoparticles by the reduction of K_2PtCl_4 with H_2 in the presence of PVP.[20,35,36] Moreover, the removal of the polymer from the surface of the nanoparticles remains difficult and can partly hamper the possibility of correlating nanomorphology with catalytic properties for supported nanostructured catalytic systems.[21]

Even if the synthesis of anisotropic Au or Ag nanorods using the seed-mediated approach was successful, the mechanism of the anisotropic growth remains unclear. The thermodynamic stabilization of given facets can be reasonably considered as the driving force for the anisotropic growth. However, other parameters were also found critical to achieve anisotropic shape. Nikoobakht et al.[37] and Gao et al.[38] proposed that the auto-organization of the CTAB molecules in a bilayer horizontal manner at the surface of the growing particle would enhance the anisotropic growth. Perez-Juste et al. explained the uniaxial growth through an electric-assisted mechanism.[39] In this case, the cationic CTAB micelles would strongly bind the $AuCl_4^-$ precursor and would transport them to the CTAB-embedded growing particle. Due to the similar positive charge on the micelles and on the growing particle, the growth rate would then be proportional to the collision frequency between these growing seeds and the CTAB−Au moieties. Moreover, since the potential profile around the particle would be easier to supersede at the extremities of the particles, anisotropic growth would be intrinsically favored. This explanation is satisfactory to describe 1-D growth but would not help to explain the formation of other nanocrystal shapes like triangular prisms or cubes. In fact, the nature of the seeds would also play a major role in directing the final shape of the growing particle.[40] Rods and wires have 5-fold symmetry and would be formed from seeds presenting five twinning planes. These decahedral particles would be formed by five tetrahedral subunits joined on their {111} facets.[41] Since the angle between the {111} facets is 70.5°, a gap of 7.5° is left. To close the gap and form a complete section, the 7.5° gap is compensated by strain effects in the lattice, resulting in twinning planes which would be preferential sites for the anisotropic growth.[42,43] This role of twin planes in generating anisotropic morphologies was also generalized to other nanocrystals like triangular prisms or hexagonal platelets.[40] At the opposite, cubes would be formed from seeds without twinning planes.[33]

The respective rates of nucleation and growth can also directly influence the morphology of the Pd nanoparticles through the so-called kinetic shape control.[44] While equilibrium nanocrystals (0-D nanoobjects) with a "rounded-like" aspect preferentially expose low-energy facets, anisotropic nanocrystals present larger surface areas and therefore metastable, high-surface-energy planes. Equilibrium nanocrystals with their low-energy facets are, therefore, formed under a thermodynamic-controlled growth regime. Such a regime is achieved in the presence of a low monomer (active atomic or molecular species) concentration during the growth step. Inversely, anisotropic nanocrystals need a high monomer concentration to achieve high-energy facets. This concept of kinetic shape control is, therefore, directly dependent on the growth rate, which depends on the monomer concentration remaining in solution. Therefore, the final nanomorphology would be the result of a balance between nucleation and growth rates which govern thermodynamics and kinetics effects. In this respect, the seed-mediated approach used in the present study would correspond to a particular case in which nucleation is governed by the amount of seeds added to the growth solution.

The objective of the present study will be to extend the seeding approach to palladium, a noble metal with important applications in catalysis. We will show that the influence of experimental conditions on the rate of reduction of the palladium precursor during the growth step strongly modifies the final morphology of the nanocrystals, bringing new information about the growth mechanism of Pd nanocrystals.

2. Experimental Section

2.1. Materials. Palladium tetrachloropalladate (Na_2PdCl_4) (98%), cetyltrimethylammonium bromide (CTAB), sodium borohydride ($NaBH_4$) (98%), L-ascorbic acid (99%), sodium ascorbate (≥98%), and sodium citrate (99%) were purchased from Sigma Aldrich. All aqueous solutions of palladium tetrachloropalladate, CTAB, $NaBH_4$, ascorbic acid, and sodium ascorbate were freshly prepared before use.

2.2. Standard Synthesis of Pd Nanoparticle Seeds. Small isotropic palladium nanoparticles (3−4 nm) were used as seeds for the growth of Pd nanostructures by reducing Na_2PdCl_4 by sodium borohydride. These seeds were prepared following the method developed by Nikoobakht and El-Sayed.[29] An amount of 50 mL of an aqueous 0.5 mM Na_2PdCl_4 solution was mixed with 25 mL of an aqueous 0.3 M CTAB solution prepared at 30 °C. Next, 6 mL of an ice-cold aqueous 0.01 M $NaBH_4$ solution was added quickly under vigorous stirring. The solution turned dark immediately after the borohydride addition, indicating metallic palladium nanoparticle formation. The palladium suspension was stirred for 15 min. The seed solution was used systematically 2 h after its preparation. This period of time is necessary for the complete decomposition of $NaBH_4$ in excess.

2.3. Synthesis of Different Pd Nanostructures. (*a) Standard Preparation*. The growth solution was obtained by mixing 50 mL of an aqueous 1.0 mM Na_2PdCl_4 solution with 50 mL of an aqueous 0.08 M CTAB solution under gentle stirring at 30 °C. After 5 min of mixing, a turbid solution was formed, indicating the formation of a CTAB−Pd complex. Next, 0.7 mL of an aqueous 0.08 M sodium ascorbate solution was then added. Finally, 60 (or 120) μL of the seed solution was injected. The initial orange-red solution changed progressively in 30 min into a dark solution, indicating the reduction of the metallic precursor.

(*b) Influence of the CTAB/Pd Molar Ratio.* An amount of 50 mL of an aqueous 1.0 mM Na_2PdCl_4 solution was mixed with 50 mL of an aqueous 0.01 or 0.08 M CTAB solution under gentle stirring at 30 °C. After 5 min of mixing, 700 μL of an aqueous 0.08 M sodium ascorbate solution was then added, followed by 60 μL of the seed solution. The initial orange-red solution turned dark in 10 min at a CTAB/Pd molar ratio of 10 and, in 30 min, at a CTAB/Pd molar ratio of 80.

(*c) Influence of the Absolute Concentration in CTAB and Na_2PdCl_4.* A series of experiments was performed at a CTAB/Pd molar ratio of 80 but with three times higher concentrated solutions for the growth step than for the standard preparation (experimental conditions were unchanged for the seed step). Therefore, 50 mL of an aqueous 3.0 mM Na_2PdCl_4 solution

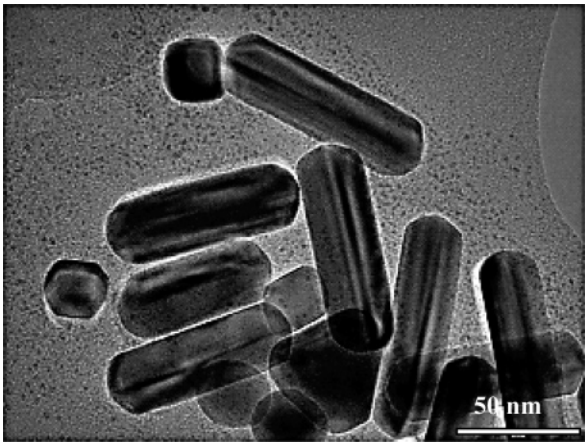

Figure 1. TEM image showing a collection of Pd nanocrystals composed mainly of nanorods but also of few "rounded" nanocubes or triangular nanosheets. The growth solution was prepared using the standard protocol with 60 μL of seeds.

was mixed with 50 mL of an aqueous 0.24 M CTAB solution under gentle stirring at 30 °C. After 5 min of mixing, 2.1 mL of an aqueous 0.08 M sodium ascorbate or ascorbic acid solution was added, followed by 360 μL of the seed solution. In the presence of sodium ascorbate, a majority of Pd nanorods was obtained.

(*d*) *Synthesis of Pd Nanocubes*. First, 50 mL of an aqueous 3.0 mM Na_2PdCl_4 solution was mixed with 50 mL of an aqueous 0.24 M CTAB solution under gentle stirring at 30 °C. Next, 2.1 mL of an aqueous 0.08 M sodium ascorbate or ascorbic acid solution was then immediately added, followed by 120 μL of the seed solution. The solution turned dark in 1 min.

(*e*) *Synthesis of Pd Icosahedra*. In order to selectively form Pd icosahedra, the procedure for the preparation of the Pd seeds had to be modified. The CTAB capping agent was, indeed, replaced by sodium citrate. Therefore, 50 mL of an aqueous 0.5 mM Na_2PdCl_4 solution was mixed with 25 mL of an aqueous 0.5 mM sodium citrate solution under gentle stirring at 30 °C. Next, 6 mL of an ice-cold aqueous 0.01 M $NaBH_4$ solution was added quickly under vigorous stirring. The solution turned dark immediately after the borohydride addition, indicating metallic palladium nanoparticle formation. The palladium suspension was stirred for 15 min. The seed solution was used 2 h after its preparation. The growth solution was prepared by mixing 50 mL of an aqueous 1.0 mM Na_2PdCl_4 solution with 50 mL of an aqueous 0.3 M CTAB solution under gentle stirring at 30 °C. After 5 min of mixing, 0.7 mL of an aqueous 0.08 M sodium ascorbate solution was then added. Finally, 120 μL of the seed solution was injected. The solution turned dark after 12 h.

2.4. X-ray Diffraction. XRD measurements were performed on a Philips PW1820 diffractometer equipped with a curved graphite monochromator using Cu Kα radiation (λ = 1.5406 Å). The Pd nanoparticle solution was obtained following the standard preparation described above. This solution was centrifuged twice at 11000 rpm for 1 h with removal of the supernatant and dilution into 100 mL of deionized water after each centrifugation step. The concentrated Pd solution was then dried at room temperature under N_2 flow before XRD analysis.

2.5. Transmission Electron Microscopy. Transmission electron microscopy studies were performed in a JEOL JEM 2010 operating at 200 kV. The microscope was equipped with an ultrahigh-resolution polar piece (point resolution, 1.9 Å). The specimens for TEM and SAED analysis were prepared by dropping and drying the colloidal solution onto a holey carbon

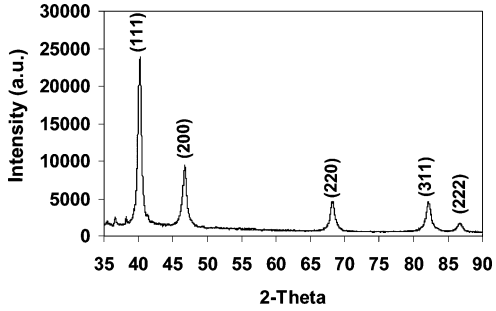

Figure 2. XRD pattern of the nanopowder obtained using the standard procedure of preparation. All diffraction peaks are assigned to the fcc bulk Pd phase.

film supported on a Cu grid (200 mesh). TEM samples were then rinsed several times with ethanol to remove the surfactant. Particle size distributions and corresponding statistical analysis of the different morphological types of nanoparticles were obtained from TEM images by using analySIS software to record digital images. In each case, at least 300−600 particles were counted on about 100 different pictures. Particular attention was paid to analyze different regions of the Cu grid without counting aggregated regions where nanoparticles tend to assemble per type of nanoobject. In order to determine the proportion of Pd involved into each type of nanoobject, yields of Pd per nanoobject were calculated taking into account their respective volumes. This yield (or volumetric percentage) was calculated according to the following equation

$$Y_j\,(\%) = \frac{\sum_i n_i v_i}{\sum_{j=1}^{n} \sum_i n_i v_i} \qquad (1)$$

with n_i, the number of particles of a given volume v_i, and j = 1,...,n, a given type of nanoobject (cubes, rods, tetrahedron, etc.).

This yield per nanoobject is, stricto sensu, different from the exact definition of yield since a small part of Pd (about 10−15%) did not react to form Pd nanoobjects and remained in solution as the metallic precursor. However, this yield per nanoobject or volumetric percentage provides useful complementary information besides the statistical distribution. Yield measurements were not reported when the proportion of triangular (or hexagonal) nanosheets was not negligible since their thickness cannot be precisely measured using TEM analysis.

2.6. UV−Vis/Near IR Measurements. The as-synthesized Pd growth solutions maintained at 30 °C were analyzed by UV−vis/near IR spectroscopy using a PerkinElmer Lambda 35 spectrophotometer in the 190−1100 nm wavelength range. Care was taken to rinse the quartz cuvette in deionized water followed by drying in a jet of nitrogen prior to each measurement.

3. Results and Discussion

3.1. The Different Kinds of Pd Nanocrystals. The seeding-mediated approach applied to palladium led to nanocrystals with well-defined nanomorphology and a very low yield of isotropic sphere-like particles, as shown Figure 1 where mainly Pd nanorods can be visualized. The XRD pattern of the as-synthesized Pd nanopowder is shown Figure 2. All diffraction peaks are in good agreement with those of the standard pattern for fcc bulk Pd metal (space group $Fm\bar{3}m$) with lattice constants $a = b = c$ = 0.389 nm (JCPDS Card No. 05-0681). The

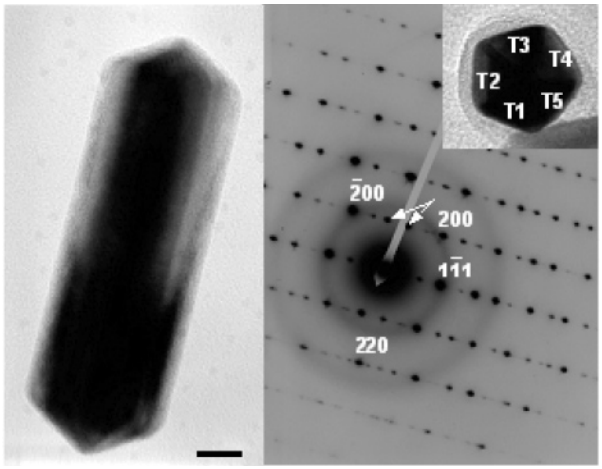

Figure 3. TEM image of a Pd nanorod (left panel; scale bar, 10 nm) and its corresponding SAED pattern (right panel). The electron diffraction pattern corresponds to a superposition of square <100> and rectangular <112> zone patterns. Arrows indicate the presence of spots resulting from double diffractions. The inset represents a cross-sectional view of the pentagonal Pd nanorod with its five tetrahedral subunits labeled as T1−T5.

respective intensities of the (111), (200), and (220) peaks are similar to those reported for fcc bulk metal due to random orientations of the different types of nanoparticles on the supporting substrate.

The TEM image of a nanorod reported in Figure 3 is consistent with a preferential elongation along a common [110] axis from an initially isometric pentatwinned seed. Each twin is formed from an elongated tetrahedron of {111} faces.[41] The inset of Figure 3 shows the pentagonal cross section of a nanorod viewed along the common [110] axis with each of the fcc tetrahedral subunits labeled as T1−T5. Due to symmetry considerations, only two Bragg diffraction orientations can be visualized; in the first case, three of the five tetrahedra are aligned along <100> (for T1) and <112> (for T3 and T4), while in the second case, three other subunits diffract along <110> (for T5) and <111> (for T2 and T3).[45] An example of an electron diffraction pattern is reported in Figure 3 (right). This pattern consists of the superposition of rectangular <112> and square <100> zones. Reflections in the square lattice due to the [001] zone correspond to ($\bar{2}$00), (020), and (220) planes. Similarly, reflections in the rectangular lattice due to the [$\bar{1}$12] zone correspond to ($1\bar{1}1$), (311), and (220) planes. Double diffraction resulting from the combination of these two crystallographic zones generates many other reflections. In the <110>/<111> zone, {111} fringes could be visualized only on one side of the rod with an angle of 55° to the common [110] axis, as reported in Figure S1. The *d* spacing was 2.3 Å close to the theoretical value of $d_{111} = 2.25$ Å. Therefore, TEM analysis confirmed that Pd nanorods obtained by the seed-mediated approach are elongated pentagonal prisms with 5 {100} side facets and 10 {111} facets at the extremities, as already observed for Au nanorods.[45]

Other shape-defined nanocrystals could often be observed during the seed-mediated preparation of Pd nanoparticles. Among them, nanocubes correspond to the smallest nanoparticles, with a size ranging between 20 and 25 nm. As shown in Figure 4, Pd nanocubes present {200} fringes with a *d* spacing of 2.0 Å (theoretical value, $d_{200} = 1.94$ Å). Moreover, the electron diffraction pattern confirms the presence of a square lattice corresponding to {100} reflections. Then, contrary to nanorods, nanocubes are single crystalline.[33]

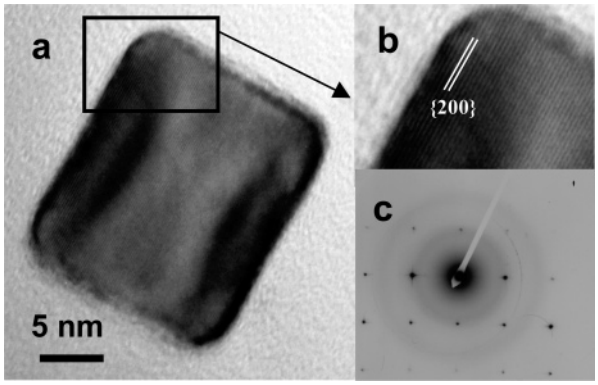

Figure 4. (a) TEM image of a Pd nanocube, (b) inset; HRTEM image of one of the corners of the nanocube showing {200} fringes running parallel to the edge, and (c) corresponding SAED pattern showing a square lattice of {200} reflections.

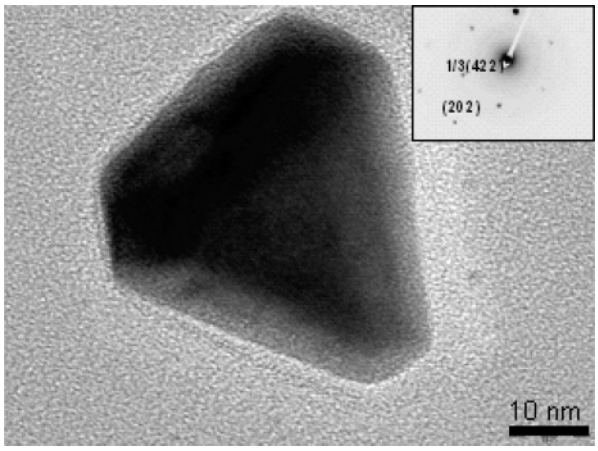

Figure 5. TEM image of a Pd triangular nanosheet with truncations at the tips. Inset: the corresponding SAED pattern showing a hexagonal pattern characteristic of the {111} facet of a fcc-packed crystal. The inner set of spots corresponds to the normally forbidden 1/3{422} reflections. These forbidden reflections are generally observed on plate-like structures and were attributed to (111) stacking faults parallel to the (111) surface.

A third family of Pd nanocrystals present a triangular aspect. However, depending on the experimental conditions used for preparing those Pd nanoparticles, the triangular aspect observed on TEM pictures could correspond either to triangular nanosheets or to a pyramidal tetrahedron. Figure 5 reports the TEM picture of one of these triangular-shaped nanoparticles with its corresponding selected-area electron diffraction pattern. This pattern is of hexagonal symmetry. Two sets of spots could be observed. The outer set of spots was indexed to {220} reflections, while the inner set of spots corresponds to the normally forbidden 1/3{422} reflections in a fcc lattice.[46−48] Such forbidden reflections indicate the presence of a plate-like structure and result from (111) stacking faults lying parallel to the surface.[49] Therefore, these triangular-shaped particles are, in fact, nanosheets with (111) lattice planes as the basal planes.

The second type of triangular-shaped nanoparticles is reported in Figure 6. These particles present a pyramid-like aspect, in agreement with a recent study by Wiley et al.[50] According to these authors, these particles would have to be more considered as tetrahedral bipyramids of Pd. As shown in Figure 6, these triangular-like particles present a rounded aspect, contrary to the straight sides of the triangular nanosheets described above. One of the particles presents a twin plane that bisects the particles into two tetrahedral halves. These bipyramid particles are, indeed, formed from single-twinned seeds. However,

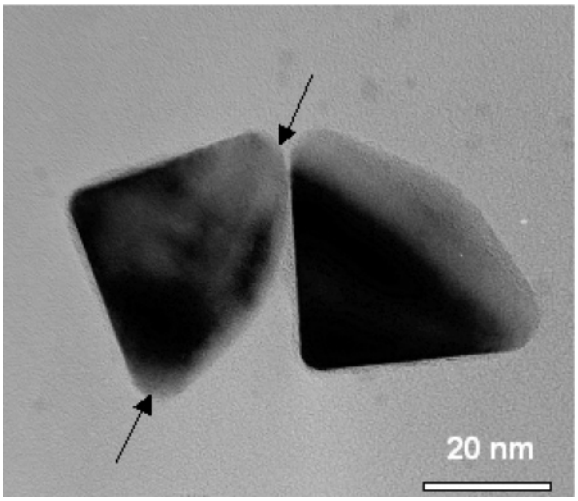

Figure 6. TEM image of right bipyramids appearing like "rounded" tetrahedral particles. A single twin plane is clearly visible (arrows) running all along one of the tetrahedral particles and bisecting it into two halves.

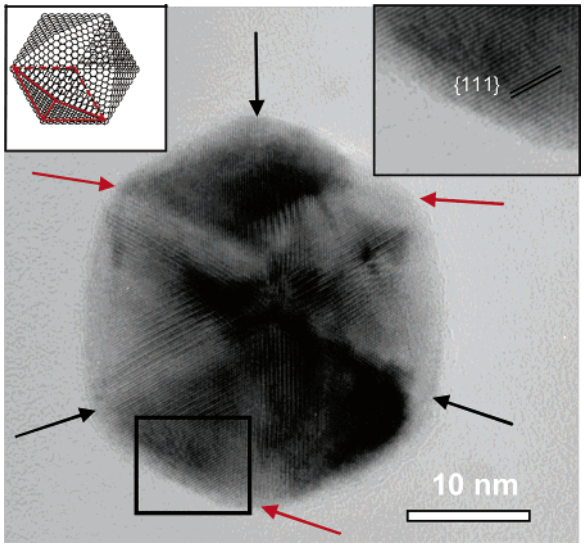

Figure 7. TEM image of an icosahedral multiply twinned Pd particle. Arrows indicates the presence of twin boundaries separating the different adjacent facets. Insets: schematic representation of an icosahedron (left) and enlarged image of the square zone area showing the presence of {111} fringes (right).

contrary to the triangular nanosheets preferentially exposing {111} facets, bipyramids would be bound by {100} facets.[50]

An important class of Pd nanocrystals is composed of icosahedral Pd nanoparticles with a mean dimension of about 30−45 nm (see Figure 7). These particles are commonly observed in TEM pictures and generally present hexagonal symmetry resulting from a 3-fold rotational axis. Even if Kuo et al.[51] ascribed their morphology to a 3-D projection of dodecahedral particles, most of the studies considered these particles as icosahedral.[52,53] Particles with icosahedron geometry present three different types of symmetry, 2-, 3-, or 5-fold. However, only the 2- or 3-fold symmetries leading to a hexagonal TEM projection can be observed since, in this case, the particles would lie flat on the grid. In the 3-fold symmetry, six twin planes would be visualized (Figure 7). These six twin planes would separate six sets of facets. Each twin plane would extend from the edge to the center of the particle along the border of two tetrahedra. However, only three of the six twinning planes (indicated by red arrows) are actually located on the side

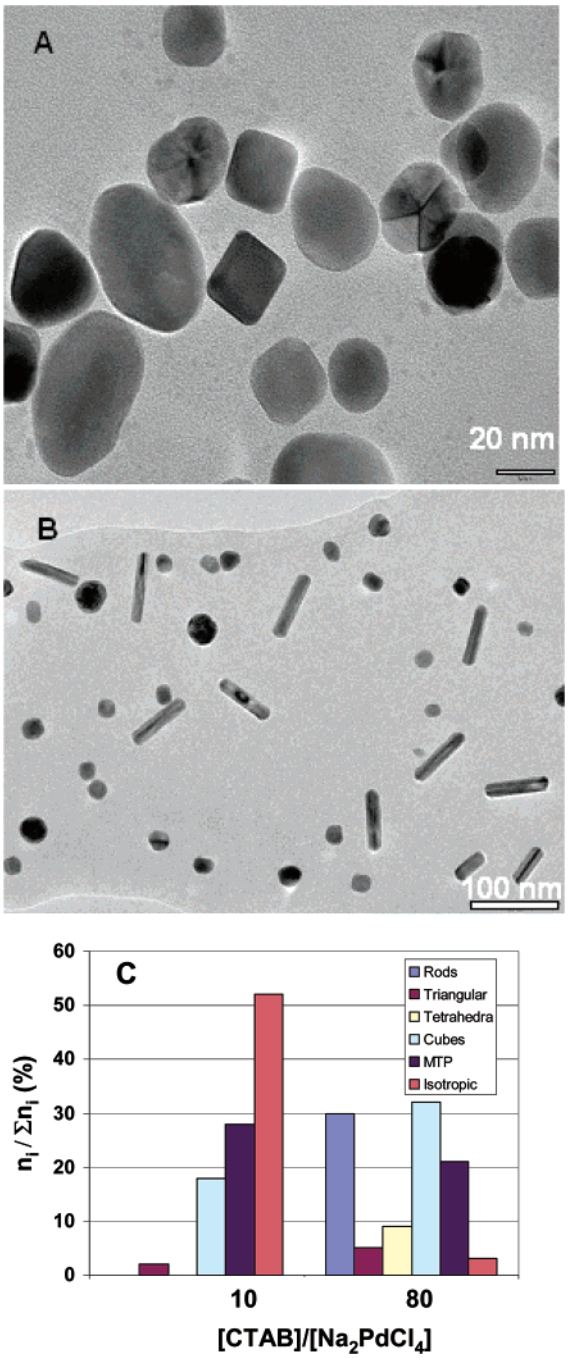

Figure 8. (A) Typical TEM image of Pd nanocrystals obtained at a $[CTAB]/[Na_2PdCl_4]$ molar ratio of 10 and (B) of 80; (C) proportions of the different types of nanocrystals obtained at $[CTAB]/[Na_2PdCl_4]$ molar ratios of 10 and 80. The tetrachloropalladate concentration remains constant at 1.0 mM.

of the surface visualized in Figure 7. Therefore, the visualization of a 6-fold symmetry of the twinning planes radiating out from a central axis is only the result of the particular icosahedral geometry. Icosahedral Pd particles are, therefore, multiply twinned particles (MTPs). An enlarged image of one of the sets of planes (square region, inset Figure 7) reveals the presence of lattice planes with a *d* spacing of 2.24 Å, corresponding to the (111) planes of fcc palladium.[52,53] Their relatively high proportion obtained in this study contrasts to the absence of pentagonal-shaped multiply twinned particles.

3.2. The Role of the CTAB Surfactant. Nanocrystal formation results from (1) a burst increase of monomer concentration up to the supersaturation ratio initiating nucleation

TABLE 1: Dimensions in nm of the Different Types of Pd Nanocrystals Formed at a Molar Ratio [CTAB]/[Na_2PdCl_4] of 10 and 80 for the Growth Step[a]

[CTAB]/[Na_2PdCl_4]	10	80
rods		$L = 63 \pm 5$ $D = 24 \pm 1$ AR $= 2.7 \pm 0.3$
cubes	21 ± 3	20 ± 3
MTPs	27 ± 2	38 ± 3
triangular	30 ± 1	39 ± 2
tetrahedral		40 ± 3
isotropic	27 ± 4	

[a] Experimental conditions for the growth step: 50 mL of 1.0 mM Na_2PdCl_4, 50 mL of 0.01 or 0.08 M CTAB, 0.7 mL of 0.08 M sodium ascorbate, 60 μL of seeds.

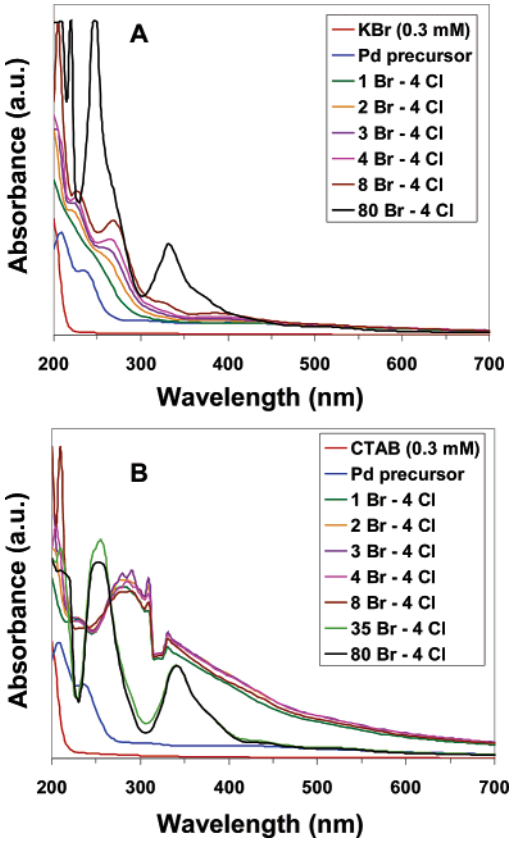

Figure 9. Progressive evolution of the UV−vis absorption spectra of Na_2PdCl_4 upon the addition of KBr (A) and upon the addition of cetyltrimethylammonium bromide (CTAB) (B). The legends indicate the relative molar concentrations of the tetrachloropalladate salt and of the KBr or CTAB. The tetrachloropalladate concentration remains constant at 0.3 mM.

and (2) a consumption of the monomers remaining in solution and participating in the growth of the seeds. In the seeding approach, this growing step can be controlled by structure-directing agents selectively inhibiting the crystalline growth along a given direction or by a proper choice of experimental conditions favoring a thermodynamic- or kinetic-controlled growth regime. In the following work, we will show that, if the rate of reduction of $PdCl_4^{2-}$ is sufficiently retarded, the growing step will turn into a kinetically controlled growth regime favoring more anisotropic shapes like 1-D nanorods or 2-D nanodisks.[54,55] This kinetic regime would result from the presence of, still, a high monomer concentration remaining in solution during the main part of the growth step.[44] On the contrary, initially increasing the rate of reduction of $PdCl_4^{2-}$ leads to a low monomer concentration in solution during the

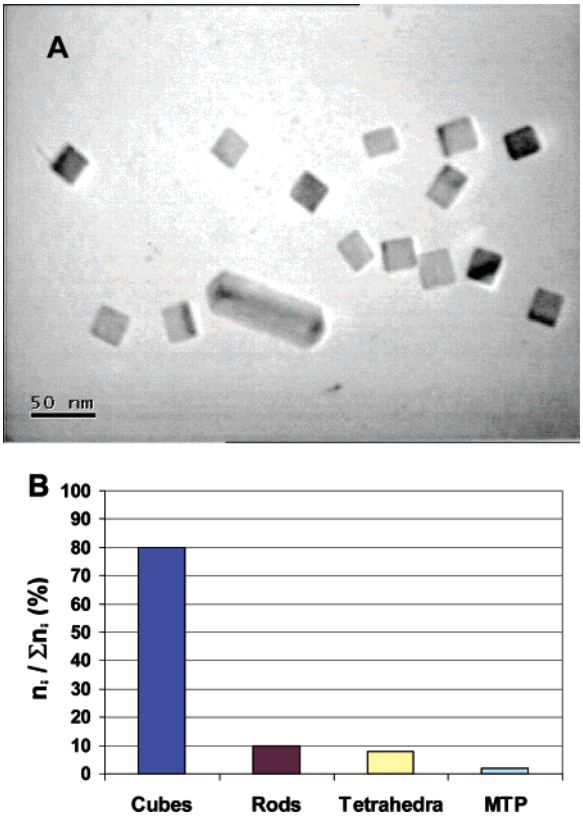

Figure 10. (A) TEM image showing a very high proportion of Pd nanocubes (size, 27 ± 4 nm) when the reducing agent and seeds are added immediately after the CTAB surfactant and the tetrachloropalladate, Na_2PdCl_4, precursor without waiting for the embedding of the palladium precursor inside CTAB micelles. (B) Histogram showing the different proportions of Pd nanocrystals. Cubes are formed in a high proportion, 80%.

main part of the growth step. For Pd nanocrystals, this would leave no other choice than to grow into a thermodynamically favored shape like cubooctahedra or multiply twinned particles (MTPs).

In this respect, the cetyltrimethylammonium bromide (CTAB) surfactant is considered to play a key role as a "complexing agent" and/or as a structure-directing agent through stabilization of {100} facets and/or through auto-organization as a bilayer. The first parameter studied was then the surfactant/metallic precursor molar ratio. Figure 8 reports two different TEM pictures at a CTAB/Na_2PdCl_4 molar ratio of 10 (A) and 80 (B) (using 60 μL of seeds). It should be first underlined that, in both cases, only the surfactant concentration was changed, while the Na_2PdCl_4 concentration remained constant at 1.0 mM. Moreover, the CTAB concentration in the growth solution was always much higher than the cmc value (0.8 mM), showing that CTAB micelles were formed in both cases. As shown in Figure 8, a dramatic change can be observed about the nanomorphology of the final Pd nanocrystals. For the CTAB/Na_2PdCl_4 molar ratio of 10, nanorods are absent on the TEM images, whereas mostly isotropic or shapeless particles are observed. Icosahedral multiply twinned particles and nanocubes are also present in a large proportion. Statistical analysis (Figure 8C and Table 1) confirmed that isotropic (or shapeless) nanoparticles represent 52% of the nanoobjects with a mean dimension of 27 ± 4 nm, multiply twinned particles represent 28% (mean size, 27 ± 2 nm), nanocubes represent 18% (mean size, 21 ± 3 nm), while very few triangular-shaped particles (~2%) are observed.

TABLE 2: Elemental Analysis Results of the Precipitates Formed by "Complexation" between CTAB and Na_2PdCl_4 at Different Molar Ratios and Relative Proportions of Bromide and Chloride in the Final Precipitate and in the Initial Solution

[CTAB]/[Na_2PdCl_4]	stoichiometric Pd/Cl/Br ratios of the precipitates	$([Br]/[Cl])_{precipitate}/([Br]/[Cl])_{solution}$
0.25	1.0:2.0:0.4	2.0
0.75	1.0:1.2:2.1	2.3
1.25	1.0:0.6:3.4	4.5

This situation differs strikingly from the one observed at a CTAB/Na_2PdCl_4 molar ratio of 80. In this case, quite anisotropic Pd nanorods were observed with a mean length of 64 ± 5 nm, a mean diameter of 24 ± 1 nm, and an aspect ratio of 2.7 ± 0.3. Moreover, statistical analysis did not show any correlation between the aspect ratio and the length of the nanorods. In other words, longer nanorods are not necessarily wider. This suggests that radial and longitudinal growth of the nanorods did not symmetrically happen.[56] Their proportion reached 30%. This was accompanied by a strong decrease in the percentage of isotropic particles. Similarly, the proportion of nanocubes increased but to a less extent, from 18 (CTAB/Pd = 10) to 32% (CTAB/Pd = 80). However, according to Table 1, their dimension remained almost unchanged at about 20 nm. Therefore, the increasing concentration of CTAB seemed to improve the formation of nanocubes. However, their yield of formation was less sensitive to the variation of the CTAB/Pd molar ratio than for nanorods. The proportion of triangular nanosheets remained in a low proportion (2−5%), while tetrahedral bipyramid nanoparticles were formed only at a CTAB/Pd molar ratio of 80. The proportion of multiply twinned particles decreased slightly from 28 to 21%, while their size increased from 27 ± 4 to 38 ± 3 nm.

Cetyltrimethylammonium bromide was recognized by Perez-Juste et al. to drastically retard the rate of metallic particle formation.[39] In the present case, at a CTAB/Pd molar ratio of 10, the solution turned dark in 10 min, while at a CTAB/Pd molar ratio of 80, the color changed progressively to a dark solution in 30 min. The increase of the CTAB concentration led to a drastic decrease of the rate of reduction of the Pd precursor. This lower reduction rate turned the growth regime into a kinetic control through the existence of, still, a high proportion of monomers in solution during the main part of the growth step. The final nanomorphology then shifted from a thermodynamically favored shape (MTPs, isotropic) to a range of shapes that deviate from those expected thermodynamically (mainly rods).

This strong decrease of the rate of reduction of the metallic precursor is related to a strong interaction between CTAB and the tetrachloropalladate salt leading to $PdBr_4^{2-}$-like moieties. The stability constant of $[PdBr_4]^{2-}$ is about 10^4 times higher than that of $[PdCl_4]^{2-}$.[57] This can be clearly observed when analyzing precipitates formed by mixing CTAB and Na_2PdCl_4 (Table 2). At a [CTAB]/[$PdCl_4^{2-}$] ratio of 1.25, the resulting stoichiometry of the precipitate was $PdCl_{0.6}Br_{3.4}$. Since the surfactant concentration was, in our preparation, in a very large excess, the exchange ligand process between Br^- and Cl^- led to completion, resulting in a final $[C_{16}TA]_2PdBr_4$ composition. This result was corroborated following the progressive replacement of the chlorine ligand by bromine using UV−vis spec-

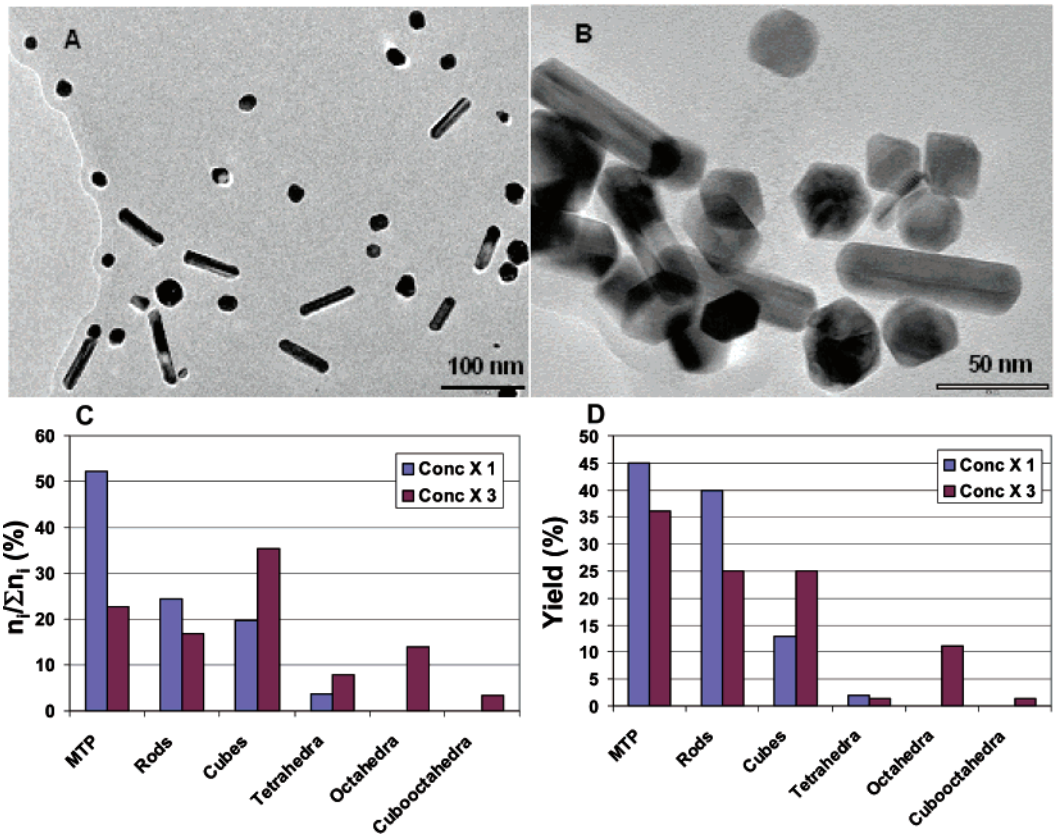

Figure 11. (A) and (B) TEM images of Pd nanocrystals obtained when increasing the concentration of Na_2PdCl_4, CTAB, ascorbic acid, and seeds three times (growth solution in A: 50 mL of 1.0 mM Na_2PdCl_4, 50 mL of 0.08 M CTAB, 0.7 mL of 0.08 M ascorbic acid, 120 μL of seeds). (C) Frequency and (D) yield (or volumetric percentage) of the different types of Pd nanocrystals.

TABLE 3: Dimensions in nm of the Different Types of Pd Nanocrystals Obtained at a CTAB/Pd Molar Ratio of 80 during the Growth Step Using the Indicated Proportions of Na_2PdCl_4, CTAB, and Reducing Agents[a]

Na_2PdCl_4	CTAB	Reducing Agent	Dimensions (nm)					
			rods	cubes	MTPs	triangular	tetrahedral	octahedra
50 mL, 1.0 mM	50 mL, 0.08 M	ascorbic acid, 0.7 mL, 0.08 M	$L = 61.6 \pm 11.0$ $D = 14.7 \pm 1.1$ AR = 4.2 ± 0.8	17.1 ± 2.3	23.1 ± 3.7	24.0 ± 1.1		
50 mL, 3.0 mM	50 mL, 0.24 M	ascorbic acid, 2.1 mL, 0.08 M	$L = 71.9 \pm 4.0$ $D = 22.4 \pm 2.6$ AR = 3.3 ±0.7	32.6 ± 3.1	41.9 ± 4.8		29.0 ± 3.8	36.7 ± 4.4
50 mL, 3.0 mM	50 mL, 0.24 M	ascorbate, 2.1 mL, 0.08 M	$L = 69.7 \pm 7.8$ $D = 24.3 \pm 1.5$ AR = 2.9 ± 0.4	16.2 ± 2.1	31.3 ± 8.7	31.5 ± 5.5	41.1 ± 2.6	

[a] The amount of seeds was adjusted (120 or 360 μL of seeds) to maintain a constant CTAB/seed ratio.

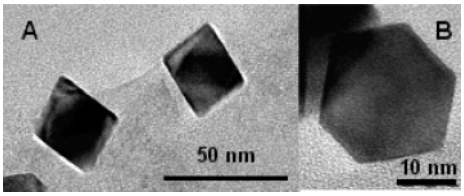

Figure 12. TEM images of (A) octahedral Pd particles and of (B) a Pd cubooctahedron.

TABLE 4: Statistical and Volumetric Distributions (Yield) of the Different Types of Pd Nanocrystals Using the Following Conditions for the Growth Step: 50 mL of 3.0 mM Na_2PdCl_4, 50 mL of 0.24 M CTAB, 2.1 mL of Sodium Ascorbate, and 360 μL of Seeds

shape	$(n_i/\sum_i n_i)$ (%)	$(v_i/\sum_i v_i)$ (%)
cubes	15	3
rods	47	74
MTPs	23	15
triangular	11	5
tetrahedral	5	3

troscopy. The $[PdCl_4]^{2-}$ species presented two absorption maxima in the UV region at 210 and 235 nm (Figure 9A). With the addition of KBr, the position maxima progressively red-shifted, and at a $[CTAB]/[PdCl_4^{2-}]$ ratio of 80, the band maxima were observed at 250 and 330 nm, which correspond to $[PdBr_4^{2-}]$.[58] Using CTAB instead of KBr led to a more rapid red-shift of the band maxima to 285 nm (Figure 9B). This pronounced red-shift compared to that of Na_2PdBr_4 is due to a strong interaction between $C_{16}TA^+$ and $PdBr_4^{2-}$. As the surfactant concentration gradually exceeded the cmc value, the absorbance at 285 nm disappeared, and new band maxima appeared at 250 and 340 nm, which were attributed to the embedding of the anion−surfactant aggregate into micelles of CTAB. The incorporation of these aggregates into CTAB micelles led to a further stabilization of the metallic precursor and to a slower reduction rate.

The importance of the preliminary embedding of the anion−surfactant aggregates into micelles of CTAB can be demonstrated using a counter experiment. If the reducing agent and seeds were added to the solution containing CTAB and the metallic precursor without waiting for the embedding of the anions into the CTAB micelles (the solution then becomes iridescent), the solution turned dark in 1 min instead of half of an hour. TEM analysis (Figure 10A) revealed the presence of a very high proportion of cubes (80%) with a narrow size distribution (27 ± 4 nm) (Figure 10B). The relatively high rate of reduction obtained without embedding of the anion inside the CTAB micelles allowed us to obtain a thermodynamic-controlled growth regime, as expected for a 0-D nanocrystal. However, a high concentration of CTAB is also necessary to stabilize selectively {100} facets. Therefore, nanocubes were formed thermodynamically, but a high CTAB concentration was needed to favor the exposition of {100} facets. Such a result showed that it is possible, in the simplest way, to generate a very high proportion of Pd nanocubes.

3.3. Factors Increasing the Formation of Pd Nanorods. Increasing the flux of monomers during the growth induction time to obtain a kinetic-controlled regime does not necessarily mean that an increase of the absolute concentrations of metallic precursor in the growth solution at a constant $CTAB/PdCl_4^{2-}$ ratio would improve the anisotropic growth. In a series of experiments using ascorbic acid (and not ascorbate) as the reducing agent, increasing the concentration of metallic precursor, CTAB, reducing agent, and seeds three times did not result in a higher proportion of rods. Analysis of the TEM pictures (Figure 11) and of the statistics about dimensions of the different nanoobjects (Table 3) showed that the percentages of icosahedral multiply twinned particles and of nanorods decreased. Considering yields (or volumetric percentages), the same conclusion is reached even if the yield of MTPs decreased to a lesser extent than for the frequency values. For nanorods, the yield decreased from 40 to 25%, showing that the moderate increase of size (Table 3) could not compensate for the lower frequency obtained from the TEM pictures. Interestingly, while the length of the nanorods slightly increased (from 62 ± 11 to 72 ± 14 nm), their diameter increased much more (from 15 ± 1 to 22 ± 3 nm). Such an increase could be related to an unselective supply of matter due to a poor stabilization effect of CTAB on the lateral sides of the nanorods. However, the main effect due to the increase of the absolute concentrations of precursors and CTAB is a high proportion of cubes (36%). Since cubes are formed in a thermodynamic regime in the presence of a high CTAB concentration, such a result could be reasonably expected. However, cubes are also formed when CTAB does not play its role of retarding agent for the reduction rate by embedding the precursor into micelles. Therefore, this result underlines the poor stabilization effect of CTAB since, at a high metallic precursor concentration, CTAB is unable to satisfactorily stabilize the $PdCl_4^{2-}$ species.

Interestingly, a low proportion of unusual morphologies was obtained under these experimental conditions. Octahedral-shaped particles were formed (frequency, 14%) with a size of 37 ± 4 nm. These octahedron particles viewed along the [110] zone axis (Figure 12A) would be covered, ideally, with {111} faces.[59] Similarly, an even lower proportion of cubooctahedra particles was detected. These particles would be formed by four {111} and two {100} facets (Figure 12B). Their existence confirmed a thermodynamic regime of growth. If CTAB really stabilizes {100} facets selectively, this would suggest that, at high CTAB concentration, the difference of stabilization between {100} and

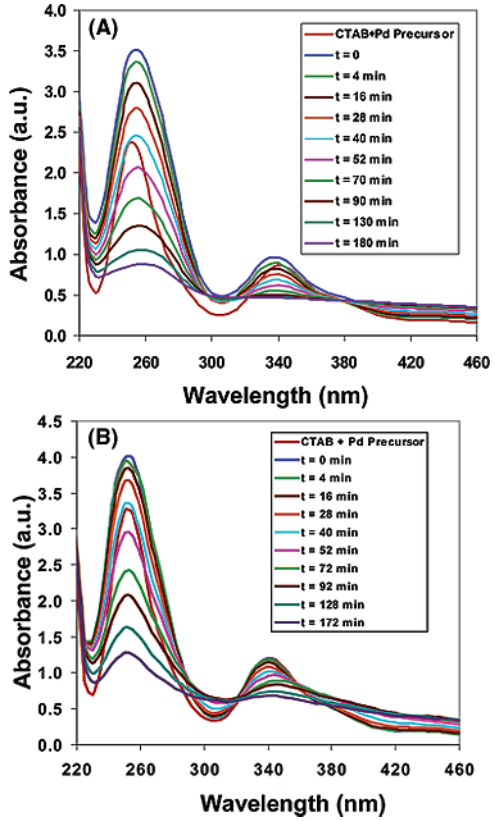

Figure 13. Evolution of the UV−vis spectra of the $PdCl_4^{2-}$ species embedded in CTAB micelles during the growth process using (A) ascorbate or (B) ascorbic acid (growth conditions: 50 mL of 0.3 mM Na_2PdCl_4, 50 mL of 0.024 M CTAB, 2.1 mL of 8 mM sodium ascorbate or ascorbic acid, 36 μL of seeds).

{111} facets through the selective adsorption of CTAB was leveled off. CTAB would then also stabilize {111} faces under these conditions but to a much less extent. It should be emphasized that the thermodynamic growth regime was achieved here due to a poor stabilization effect of CTAB, not to a too fast initial consumption of monomers, making possible a thermodynamic growth of some of the nanoobjects. However, these experimental conditions are less effective in producing thermodynamic-shaped particles since rods were also formed. Therefore, increasing the reduction rate is a better way to selectively shift the regime to thermodynamic conditions.

The same series of experiments performed in the presence of ascorbate instead of ascorbic acid shifted the growth process to a more efficient kinetic control (Table 4). This change of the nature of the reducing agent dramatically modified the relative proportions of the different nanoobjects. While the kinetically controlled nanorods increased from 24 to 47%, thermodynamically controlled nanoobjects like cubes or hexagonal-like particles were formed in a lower proportion (from 20 to 15% for cubes and from 52 to 23% for icosahedral MTPs). Considering their respective volumetric percentages (or yields), variations were more marked since, for cubes, the yield dramatically decreased from 25 to 3%, while for MTPs, it decreased from 45 to 15%. Inversely, a marked increase was found for rods since the yield changed from 40 to 74%. This result could appear surprising since ascorbate is known to be a stronger reducing agent than its acidic form, ascorbic acid. Such a modification would then be unfavorable to obtain a better kinetic regime. Figure 13 reports the evolution of the UV−vis spectra of the CTAB−$PdCl_4^{2-}$ mixture in the presence of ascorbate (A) or ascorbic acid (B) during the growth step after the injection of

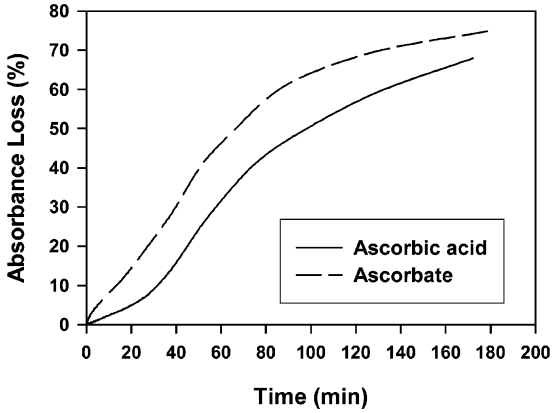

Figure 14. Evolution of the absorbance loss of the UV band at 250−265 nm of the $PdCl_4^{2-}$ species embedded in CTAB micelles during the growth process (growth conditions: 50 mL of 0.3 mM Na_2PdCl_4, 50 mL of 0.024 M CTAB, 2.1 mL of 8 mM sodium ascorbate or ascorbic acid, 36 μL of seeds).

the Pd seeds. Results confirmed a higher rate of disappearance of the $PdCl_4^{2-}$ UV signal at 250−265 nm using ascorbate. This result was confirmed by reporting the percentage of absorbance loss using both reducing agents (see Figure 14). This acceleration of the reduction rate is, however, quite moderate; 2 h after the injection of the Pd seeds, the absorbance loss increased by only about 10% using ascorbate. Therefore, significantly, this effect cannot be considered as the unique decisive factor influencing the growth regime. In fact, since CTAB is a cationic surfactant and the micelles are positively charged, a stronger interaction is expected between ascorbate and the cationic micelles in which the $PdCl_4^{2-}$ precursor is embedded. This can be clearly observed by comparing the UV−vis spectra for the CTAB−ascorbic acid and CTAB−ascorbate mixtures (see Figure S2). The interaction between CTAB and ascorbate led to a red-shift (from 255 to 265 nm) of the main UV band of vibration. This stronger interaction would favor the reduction of the $PdCl_4^{2-}$ species inside the CTAB micelles. This would enhance a better control of the adjunction of monomers by CTAB to the growing particles. If such an explanation is correct, a lower concentration of CTAB would level off differences between ascorbic acid and ascorbate due to a less favorable ascorbate−CTAB interaction, other parameters remaining equal. This was confirmed by comparing the respective influences of ascorbic acid and ascorbate at a CTAB concentration of 0.035 M instead of 0.08 M. Figure 15A and B represents a typical collection of nanocrystals obtained in the presence of ascorbic acid or ascorbate, respectively. Table 5 reports the average dimensions for each type of nanocrystal in both cases. The average length of the nanorods decreased significantly from 66 ± 13 to 46 ± 3 nm, while their diameters increased from 15 ± 1 to 21 ± 1 nm. Such an effect is expected when changing from ascorbic acid to ascorbate due to the higher reducing character of ascorbate. For other types of nanoobjects, size variations were very limited. Analysis of the frequency variations (Figure 15C) did not evidence changes in the respective proportions of nanocrystals. Icosahedral, cubic, and isotropic particles represent a large proportion of the nanoobjects formed, while the percentage of nanorods decreased slightly (from 23 to 18%). Therefore, in the present case, ascorbate did not interact efficiently with CTAB. Moreover, the high proportion of cubes and isotropic particles (absent at a CTAB concentration of 0.08 M) emphasizes a lower efficiency of CTAB for embedding $PdCl_4^{2-}$ moieties inside micelles. The lower aspect ratio of the as-obtained nanorods also suggests a lower stabilization effect

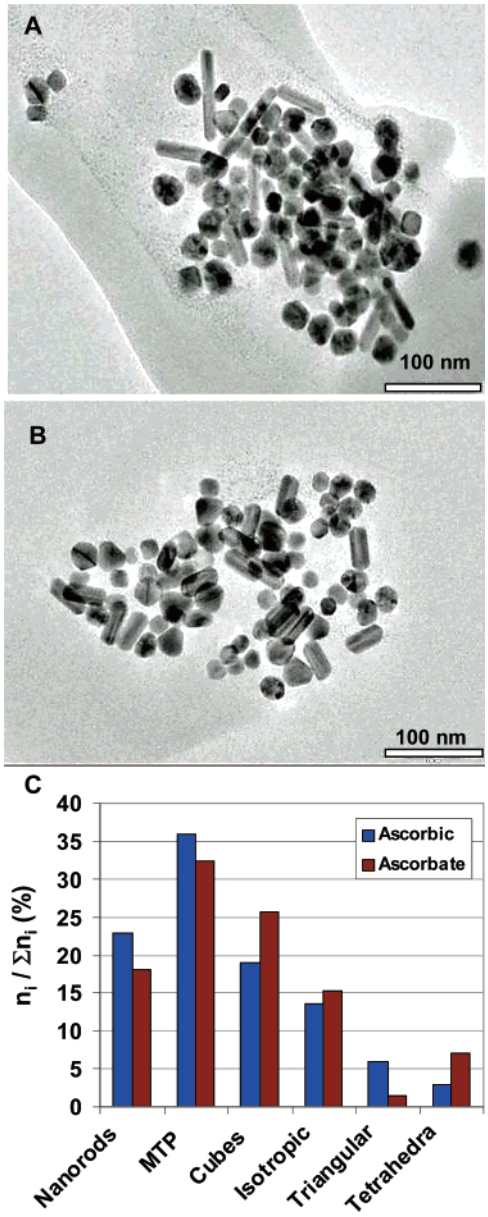

Figure 15. TEM images of Pd nanocrystals obtained in the presence of (A) ascorbic acid or (B) ascorbate at a CTAB concentration of 0.035 M (growth solution: 50 mL of 1.0 mM Na_2PdCl_4, 50 mL of 0.035 M CTAB, 0.7 mL of 0.08 M ascorbic acid or ascorbate, 120 μL of seeds). (C) Proportions of the different types of Pd nanocrystals in the presence of ascorbic acid or ascorbate at a CTAB concentration of 0.035 M.

of CTAB, leading to a supply of monomers not only to the {111} extremities of the growing nanorods but also to the {100} lateral faces.

Therefore, the kinetically controlled formation of nanorods needs a combined stabilization of $PdCl_4^{2-}$ moieties inside CTAB micelles with a high interaction between ascorbate and the cationic surfactant in order to allow CTAB to control the rate of reduction of the Pd precursor. Moreover, it should be underlined that complementary studies showed that, contrary to gold nanorods, the addition of $AgNO_3$ did not increase the proportion of Pd nanorods.

3.4. Selective Synthesis of Icosahedral Pd Particles. If the formation of kinetically controlled nanocrystals needs a delicate adjustment of the kinetics of reduction and of stabilization effects of planes by the CTAB molecules, thermodynamically controlled nanocrystals are generally easier to obtain selectively. As noted before, the rapid initial consumption of monomers in

TABLE 5: Dimensions in nm of the Different Types of Pd Nanocrystals Obtained at a CTAB/Pd Molar Ratio of 35 in the Presence of Ascorbic Acid or Ascorbate[a]

shape	ascorbic acid	ascorbate
rods	$L = 66 \pm 13$	$L = 46 \pm 3$
	$D = 15 \pm 1$	$D = 21 \pm 1$
	AR $= 4.5 \pm 1.1$	AR $= 2.2 \pm 0.2$
cubes	20 ± 1	16 ± 4
MTPs	29 ± 2	27 ± 2
tetrahedral	26 ± 1	30 ± 1
triangular	25 ± 1	29 ± 1
isotropic	20 ± 2	21 ± 2

[a] Experimental conditions for the growth step: 50 mL of 1.0 mM Na_2PdCl_4, 50 mL of 0.035 M CTAB, 0.7 mL of 0.08 M ascorbic acid or sodium ascorbate, 120 μL of seeds.

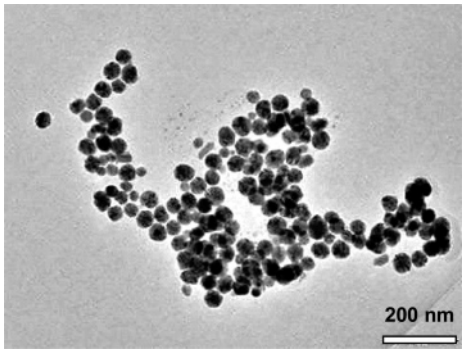

Figure 16. TEM image of a collection of icosahedral multiply twinned particles formed using citrate-capped Pd seeds.

the presence of a high CTAB concentration led to the formation of Pd nanocubes in a high yield. Inversely, thermodynamic control can also be reached by strongly decreasing the rate of monomer addition to the growing particle. Such a growth regime will favor the formation of 0-D nanocrystals, exposing low-energy facets like icosahedral palladium nanoparticles. This "restricted" growth regime can be achieved using citrate-capped palladium seeds instead of CTAB-capped ones. Since citrate is a stronger capping agent, these capped seeds will induce a slower growth regime when used in a second step in the presence of a CTAB aqueous growth solution. If this increased capping effect of seeds is combined with a higher CTAB/Pd molar ratio during the growth step, the growth rate can be sufficiently retarded, leading to a low flux of monomers. Indeed, under these experimental conditions, the growth solution was found to turn dark in 12 h instead of 30 min using the standard procedure. Figure 16 shows a typical TEM image of the Pd nanocrystals obtained under these experimental conditions. This restricted growth regime led to almost exclusively polyhedral Pd nanoparticles (~98%) with a mean size of 43 ± 6 nm. Moreover, complementary studies showed that a simple modification of the CTAB/Pd ratio in the growth step (but still using citrate-capped seeds) can be used to tune the size of these nanoparticles. For instance, reducing the CTAB/Pd ratio while maintaining constant all other experimental conditions led to the selective synthesis of icosahedral Pd nanoparticles with a mean size of 125 ± 43 nm. The lower the CTAB/Pd molar ratio, the higher the size of the icosahedral Pd particles. This result is expected since decreasing the CTAB/Pd molar ratio would lead to a less restricted growth rate and to bigger icosahedral particles. Their proportion remained quite high (89%), while only a few nanorods could be observed (11%). Such a result suggests that the final morphology is, in this case, governed mainly by the citrate capping effect of Pd seeds. Moreover, as proposed by Xiong et al.,[53] a possible blocking

of oxidative etching by citrate could help in stabilizing selectively icosahedral MTPs to the exclusion of other thermodynamically controlled nanocrystals. These results then confirmed that the nature of Pd seeds is also an important parameter governing the shape-controlled synthesis of Pd nanoparticles.

These different kinds of nanocrystals by exposing preferentially (100) or (111) crystallographic planes are good candidates to study morphology−selectivity relationships in structure-sensitive reactions like selective hydrogenations. Studies are in progress in this field to determine the influence of their respective morphology to the catalytic properties for selective hydrogenation reactions.

4. Conclusion

In summary, we have reported a seeding approach in aqueous solution to synthesize Pd nanostructures. A wide variety of morphologies can be obtained using this technique from 0-D (cubes, icosahedral multiply twinned particles) to 1-D (nanorods) and finally 2-D nanocrystals (triangular nanosheets). Formation of 1-D or 2-D nanocrystals results from a kinetically controlled growth regime. Such a kinetic control needs the embedding of the palladium precursor into CTAB micelles to sufficiently retard the rate of reduction, leading to a high monomer concentration during the main part of the growth step. Moreover, the kinetic control is better achieved if a high CTAB concentration is combined with the use of ascorbate to improve the interaction between the reducing agent and the cationic surfactant embedding palladium. However, even if CTAB is successfully applied here to form Pd nanocrystals, this cationic surfactant remains a poor capping agent, which does not allow for shifting of the formation of Pd nanocrystals into only one type of kinetically controlled nanocrystals. Further studies are then necessary to improve their homogeneity in shape.

In an opposite way, thermodynamic-controlled nanocrystals (cubes, icosahedral MTPs) could be selectively formed. Cubes are obtained in a high proportion (80%) if reduction is initiated without waiting for the embedding of the palladium precursor into CTAB micelles. Similarly, citrate-capped Pd seeds lead to the selective formation of icosahedral multiply twinned particles whose size can be tuned by simply modifying the CTAB/Pd molar ratio during the growth step.

Acknowledgment. This work was supported, in part, by the ANR ("Agence National de la Recherche") under CHESS program. G. Berhault thanks IFP for its continuous support.

Supporting Information Available: TEM image of Pd nanorods and UV−vis spectra of CTAB−ascorbic acid and CTAB−ascorbate mixtures. This material is available free of charge via the Internet at http://pubs.acs.org.

References and Notes

(1) El-Sayed, M. A. *Acc. Chem. Res.* **2001**, *34*, 257.
(2) Murphy, C. J. *Science* **2002**, *298*, 2139.
(3) Law, M.; Sibuly, D. J.; Johnson, J. C.; Goldberger, J.; Saykally, R. J.; Yang, P. *Science* **2004**, *305*, 1269.
(4) Maier, S. A.; Kik, P. G.; Atwater, H. A.; Meltzer, S.; Harel, E.; Koel, B. E.; Requichia, A. A. *Nature Mater.* **2003**, *2*, 229.
(5) Fukuoka, A.; Higashimoto, N.; Sakamoto, Y.; Inagaki, S.; Fukushima, Y.; Ichikawa, M. *Microporous Mesoporous Mater.* **2001**, *48*, 171.
(6) Chimentao, R. J.; Kirm, I.; Medina, F.; Rodriguez, X.; Cesteros, Y.; Salagre, P.; Sueiras, J. E. *Chem. Comm.* **2004**, 846.
(7) Štengl, V.; Bakardjieva, S.; Šubrt, J.; Večerníková, E.; Szatmary, L.; Klementová, M.; Balek, V. *Appl. Catal., B* **2006**, *63*, 20.
(8) Liu, F.; Lee, J. Y.; Wei, J. *Small* **2006**, *2*, 121.
(9) Huang, P. X.; Wu, F.; Zhu, B. C.; Gao, X. P.; Zhu, H. Y.; Yan, T. Y.; Huang, W. P.; Wu, S. H.; Song, D. Y. *J. Phys. Chem. B* **2005**, *109*, 19169.
(10) Huang, Y.; Duan, X.; Lieber, C. M. *Science* **2001**, *291*, 630.
(11) Sudeep, P. K.; Shibu, J. S. T.; George, T. K. *J. Am. Chem. Soc.* **2005**, *127*, 6516.
(12) Salem, A. K.; Searson, P. C.; Leong, K. W. *Nature Mater.* **2003**, *2*, 668.
(13) Huang, X.; El-Sayed, I. H.; Qian, W.; El-Sayed, M. A. *J. Am. Chem. Soc.* **2006**, *128*, 2115.
(14) Perez-Juste, J.; Pastoriza-Santos, I.; Liz-Marzán, L. M.; Mulvaney, P. *Coord. Chem. Rev.* **2005**, *249*, 1870.
(15) Liz-Marzán, L. M. *Langmuir* **2006**, *22*, 32.
(16) Nikoobakht, B.; Wang, Z.; El-Sayed, M. A. *Chem. Phys. Lett.* **2002**, *366*, 17.
(17) Gersten, J.; Nitzan, A. *J. Chem. Phys.* **1980**, *73*, 3023.
(18) Hao, E.; Schatz, G. C.; Hupp, J. T. *J. Fluoresc.* **2004**, *14*, 331.
(19) Murphy, C. J.; Sau, T. K.; Gole, A. M.; Orendorff, C. J.; Gao, J.; Gou, L.; Hunyadi, S. E.; Li, T. *J. Phys. Chem. B* **2005**, *109*, 13857.
(20) Narayanan, R.; El-Sayed, M. A. *J. Phys. Chem. B* **2004**, *108*, 5726.
(21) Telkar, M. M.; Rode, C. V.; Chaudhari, R. V.; Joshi, S. S.; Nalawade, A. M. *Appl. Catal., A* **2004**, *273*, 11.
(22) Balint, I.; Miyazaki, A.; Aika, K. *Phys. Chem. Chem. Phys.* **2004**, *6*, 2000.
(23) Grunes, J.; Zhu, J.; Somorjai, G. A. *Chem. Comm.* **2003**, 2257.
(24) Wu, Y.; Yang, P. *J. Am. Chem. Soc.* **2001**, *123*, 3165.
(25) Wang, J.; Tian, M.; Mallouk, T. E.; Chan, M. H. W. *J. Phys. Chem. B* **2004**, *108*, 841.
(26) Sau, T. K.; Murphy, C. J. *Langmuir* **2004**, *20*, 4414.
(27) Busbee, D.; O'Bare, S. O.; Murphy, C. J. *Adv. Mater.* **2003**, *15*, 414.
(28) Gole, A.; Murphy, C. J. *Chem. Mater.* **2004**, *16*, 3633.
(29) Nikoobakht, B.; El-Sayed, M. A. *Chem. Mater.* **2003**, *15*, 1957.
(30) Sun, Y.; Xia, Y. *Science* **2002**, *298*, 2176.
(31) Murphy, C. J.; Jana, N. *Adv. Mater.* **2002**, *14*, 80.
(32) Teranishi, T.; Miyake, M. *Chem. Mater.* **1998**, *10*, 594.
(33) Wiley, B.; Herricks, T.; Sun, Y.; Xia, Y. *Nano Lett.* **2004**, *4*, 1733.
(34) Xiong, Y.; Chen, J.; Wiley, B.; Xia, Y.; Yin, Y.; Li, Z. Y. *Nano Lett.* **2005**, *5*, 1237.
(35) Narayanan, R.; El-Sayed, M. A. *J. Am. Chem. Soc.* **2004**, *126*, 7194.
(36) Narayanan, R.; El-Sayed, M. A. *Nano Lett.* **2004**, *4*, 1343.
(37) Nikoobakht, B.; El-Sayed, M. A. *Langmuir* **2001**, *17*, 6368.
(38) Gao, J.; Bender, C. M.; Murphy, C. J. *Langmuir* **2003**, *19*, 9065.
(39) Perez-Juste, J.; Liz-Marzan, L. M.; Carnie, S.; Chan, D. Y. C.; Mulvaney, P. *Adv. Funct. Mater.* **2004**, *14*, 571.
(40) Lofton, C.; Sigmund, W. *Adv. Funct. Mater.* **2005**, *15*, 1197.
(41) Chen, H.; Gao, Y.; Zhang, H.; Liu, L.; Yu, H.; Tian, H.; Xie, S.; Li, J. *J. Phys. Chem. B* **2004**, *108*, 12038.
(42) Gai, P. L.; Harmer, M. A. *Nano Lett.* **2002**, *2*, 771.
(43) Zhang, S. H.; Jiang, Z. Y.; Xie, Z. X.; Xu, X.; Huang, R. B.; Zheng, L. S. *J. Phys. Chem. B* **2005**, *109*, 9416.
(44) Yin, Y.; Alivisatos, A. P. *Nature* **2005**, *437*, 664.
(45) Johnson, C. J.; Dujardin, E.; Davis, S. A.; Murphy, C. J.; Mann, S. *J. Mater. Chem.* **2002**, *12*, 1765.
(46) Kirkland, A. I.; Jefferson, D. A.; Duff, D. G.; Edwards, P. P.; Gameson, I.; Johnson, B. F. G.; Smith, D. J. *Proc. R. Soc. London, Ser. A* **1993**, *440*, 589.
(47) Germani, V.; Li, J.; Ingert, D.; Wang, Z. L.; Pileni, M. P. *J. Phys. Chem. B* **2003**, *107*, 8717.
(48) Salzemann, C.; Urban, J.; Lisiecki, I.; Pileni, M. P. *Adv. Funct. Mater.* **2005**, *15*, 1277.
(49) Li, C.; Cai, W.; Li, Y.; Hu, J.; Liu, P. *J. Phys. Chem. B* **2006**, *110*, 1546.
(50) Wiley, B. J.; Xiong, Y.; Li, Z. Y.; Yin, Y.; Xia, Y. *Nano Lett.* **2006**, *6*, 765.
(51) Kuo, C.-H.; Chiang, T.-F.; Chen, L.-J.; Huang, M. H. *Langmuir* **2004**, *20*, 7820.
(52) Yuan, J.; Chen, Y.; Han, D.; Zhang, Y.; Shen, Y.; Wang, Z.; Niu, L. *Nanotechnology* **2006**, *17*, 4689.
(53) Xiong, Y.; McLellan, J. M.; Yin, Y.; Xia, Y. *Angew. Chem., Int. Ed.* **2007**, *46*, 790.
(54) Mullin, J.W. *Crystallization*; Butterworth: London, 1961.
(55) Washio, I.; Xiong, Y.; Yin, Y.; Xia, Y. *Adv. Mater.* **2006**, *18*, 1745.
(56) Liao, H.; Hafner, J. H. *J. Phys. Chem. B* **2004**, *108*, 19276.
(57) Srivastava, S. C.; Newman, L. *Inorg. Chem.* **1966**, *5*, 1506.
(58) Veisz, B.; Kiraly, Z. *Langmuir* **2003**, *19*, 4817.
(59) Song, Y.; Kim, F.; Connor, S.; Somorjai, G. A.; Yang, P. *J. Phys. Chem. B* **2005**, *109*, 188.